Effect of Blasting Treatments on the Surface Topography and Cell Adhesion on Biodegradable FeMn-Based Stents Processed by Laser Powder Bed Fusion

Birgit Paul, Anja Hofmann, Sönke Weinert, Frieda Frank, Ulrike Wolff, Maria Krautz, Jan Edelmann, Michael W. Gee, Christian Reeps, and Julia Hufenbach*

Despite all progresses made so far, in-stent restenosis (ISR) is still a vital problem after angioplasty and stenting with permanent stents. Therefore, the effects of microblasting on laser powder bed fusion (LPBF) manufactured biodegradable Fe-based stents with regard to surface topography and its effect on smooth muscle cell (SMC) adherence, which could be interpreted as an early hallmark for ISR, are characterized. The LPBF-processed Fe-30Mn-1C-0.025S stents are microblasted with spherical glass beads and angular corundum particles. On the microscale, the partially molten particles on the stents are significantly reduced after the surface treatments, especially after microblasting with glass beads. Angular corundum particles lead to a rougher surface on the nanoscale as demonstrated by scanning electron microscopy and atomic force microscopy. With the aim to reduce migration and proliferation of SMC, which contribute to ISR after stenting, the interactions of microblasted stent surfaces with SMC are assessed by fluorescence microscopy. Both microblasted surfaces reduce SMC adhesion and change SMC morphology compared to the as-built state as well as to commercially available 316L stents. In conclusion, microblasting treatment shows a high potential for the postprocessing of additively manufactured, biodegradable stents due to the reduction of the surface roughness and possible beneficial effect regarding ISR.

1. Introduction

Additive manufacturing (AM) allows the fabrication of customized implants. Especially the processing of alloys by laser powder bed fusion (LPBF), the dominating technology in metal AM presents an efficient way to generate implants with complex geometries and functional integration.[1–3] Besides these advantages, rapid cooling rates, occurring during the process, promote, e.g., grain refinement, extended solid solubility, and a reduction of quantity and size of phase segregations, which result in different microstructural characteristics compared to conventional processing routes.[4,5]

LPBF has been investigated intensively for nondegradable implant materials.[1,3,6,7] However, biodegradable alloys are of increasing interest for temporary implant applications.[8–11] After healing of the damaged or diseased tissue, the temporary mechanical support of such biodegradable implants will slowly decrease, while degradation occurs without the release of toxic

B. Paul, U. Wolff, M. Krautz, J. Hufenbach
Leibniz Institute for Solid State and Materials Research Dresden
Helmholtzstraße 20, 01069 Dresden, Germany
E-mail: j.k.hufenbach@ifw-dresden.de

A. Hofmann, F. Frank, C. Reeps
Division of Vascular and Endovascular Surgery
Department for Visceral, Thoracic and Vascular Surgery
Medical Faculty Carl Gustav Carus and University Hospital Carl Gustav Carus Dresden
Technische Universität Dresden
Fetscherstraße 74, 01307 Dresden, Germany

The ORCID identification number(s) for the author(s) of this article can be found under https://doi.org/10.1002/adem.202200961.

S. Weinert
Department of Internal Medicine
Division of Cardiology and Angiology
Otto-von-Guericke University
Leipziger Straße 44, 39120 Magdeburg, Germany

J. Edelmann
Functional Surfaces and Micro Manufacturing
Fraunhofer Institute for Machine Tools and Forming Technology
Reichenhainer Straße 88, 09126 Chemnitz, Germany

M. W. Gee
School of Engineering and Design
Technische Universität München
Parkring 35, 85748 Garching b. München, Germany

J. Hufenbach
Institute of Materials Science
Technische Universität Bergakademie Freiberg
Gustav-Zeuner-Straße 5, 09599 Freiberg, Germany

**ADVANCED
SCIENCE NEWS**

www.advancedsciencenews.com

**ADVANCED
ENGINEERING
MATERIALS**

www.aem-journal.com

compounds.[12,13] Nevertheless, only few studies on LPBF manufacturing of biodegradable Mg-, Fe-, and Zn-based alloys for applications in hard or soft tissues exist.[14–21] Especially, biodegradable FeMn-based alloys are attractive for this processing method due to their excellent processability, attractive mechanical properties, and a high mechanical integrity during degradation and a good biocompatibility.[21–23] These alloys are of high interest with regard to filigree, biodegradable stent structures to overcome clinical complications of permanent stents, like in-stent restenosis (ISR), stent thrombosis (ST), or chronic inflammation.[24,25] ISR is the gradual renarrowing of previously stented areas due to, e.g., atherosclerotic plaque or neointimal proliferation, while ST is the sudden formation of a thrombus inside the stent.[26]

Cellular responses after stent placement are divided into four phases: thrombosis, inflammation, proliferation, and remodeling.[27] In the early phase, a thrombus forms due to platelet adhesion, while simultaneously inflammatory processes occur that are caused by endothelial denudation and injury of the vessel wall. Then activated endothelial and inflammatory cells release growth factors and cytokines, and thereby stimulating the proliferation of endothelial and smooth muscle cells (SMC), promoting a vicious cycle. In the remodeling phase, SMC undergo phenotypic changes that are needed for migration and proliferation, which could encourage ISR at the excessive level. At this stage, SMC produce large amounts of extracellular matrix thereby facilitating the remodeling of the vessel wall.[27–29] A challenging issue in novel stent technologies is the development of materials and surfaces that stimulate endothelial cell adhesion and proliferation but simultaneously prevent SMC adhesion, migration, and proliferation.[30]

One of the major challenges of LPBF is a defined surface roughness. The surface exhibits a process-immanent higher roughness after processing due to, e.g., partially molten particles, which can cause stress concentrations under loading initiating cracks.[31,32] It can be influenced by the LPBF processing parameters, e.g., laser power, hatch distance, laser scanning velocity, as well as powder morphology, composition, or particle size distribution.[33–35] However, a smooth surface is of great importance for applied stents, which is conventionally realized by chemical treatment after laser cutting.[36] The low roughness is especially important during stent placement to reduce the injury of endothelial cells and activation of SMC, thus to prevent ISR. In addition, the surface roughness of the LPBF-processed stent might result in a damage of the inflating balloon catheter. For postprocessing of LPBF-processed components, chemical (e.g., electrochemical polishing), physical (e.g., thermal spraying), or mechanical methods (e.g., blasting treatments, milling) are applied.[37–40] The mechanical method of blasting is thereby widespread as first postprocessing step after the LPBF process.[32,37] It will introduce residual compressive stress in the component surface due to plastic deformation, which has a positive effect on, e.g., hardness, fatigue, and tensile strength, as seen for other bulk materials.[41,42]

Pure iron stents are known for their low degradation rates. However, addition of 30 wt% manganese increases the degradation rate in vitro up to ≈70%. This could be further increased in the Fe-30Mn-1C-0.025S (FeMnCS) alloy, which has been developed by our group.[43,44] Indirect in vitro tests with fibroblasts

confirmed the cytocompatibility of the material. It was further demonstrated that endothelial cells survived up to 14 days under static conditions on as-built LPBF-processed FeMnCS generic stent structures.[45] However, it was shown that vascular cells favor the smoother parts of the stent surfaces, in between the partially molten powder particles. Therefore, smoothening of the surface might be essential for cell growth and affect SMC and endothelial cells in a different way.[46] Besides cellular response, clinical implants of a degradable alloy need a smooth surface and a homogeneous surface morphology to enable a uniform and controlled degradation. A balance of those different aspects regarding implant surface has to be found. Surface treatment of biodegradable Fe-based alloys is a critical step and novel treatment protocols, e.g., by mechanical methods, have to be established. In this preliminary study, the influence of microblasting with glass beads or corundum particles on the surface roughness, morphology, and surface elemental composition of LPBF-processed biodegradable FeMnCS generic stent structures is presented as well as its influence on SMC adhesion.

2. Experimental Section

As described previously,[18] spherical powders with a nominal composition of 68.98 wt% Fe, 30 wt% Mn, 1 wt% C, and 0.02 wt% S (FeMnCS) were used in LPBF process (SLM 250HL with a 400 W Yb:YAG laser, SLM solution) to manufacture stent structures. A point exposure strategy with a laser power of 100 W and an exposure time of 400 μs was applied. The spot size was set to 80 μm and the layer thickness to 30 μm, while the processing chamber was flooded with argon.

Stent surfaces were treated with microblasting using 5 bar and glass beads (0–50 μm; Hasenfratz Sandstrahltechnik) or white corundum (Al_2O_3) F600 (9.3 μm; Hasenfratz Sandstrahltechnik), whereby each stent was treated separately. Their composition is summarized in **Table 1**. Scanning electron microscopy (SEM; EVO MA 25, Carl Zeiss Microscopy GmbH) images of the different blasting materials are shown in **Figure 1**. For this SEM image, glass beads were sputtered with Au.

The surface topographies of the microblasted stents were analyzed by atomic force microscopy (AFM; Dimension Icon, Bruker). Images were obtained in the tapping mode with a scan rate of 0.5 Hz. The root mean squared roughness (R_q) was used to evaluate the surface roughness based on a 20×20 μm² scan area. A VHX-7000 (Keyence) was utilized to analyze stent

Table 1. Composition of glass beads and corundum particles used for microblasting according to the manufacturer.

Composition glass beads		Composition corundum particles	
SiO_2	70–75%	Al_2O_3	99.69%
Na_2O	12–15%	Na_2O	0.20%
CaO	7–12%	Fe_2O_3	0.02%
MgO	max. 5.0%	SiO_2	0.03%
Al_2O_3	max. 2.5%	CaO	0.05%
K_2O	max. 1.5%	TiO_2	0.01%
Fe_2O_3	max. 0.5%		
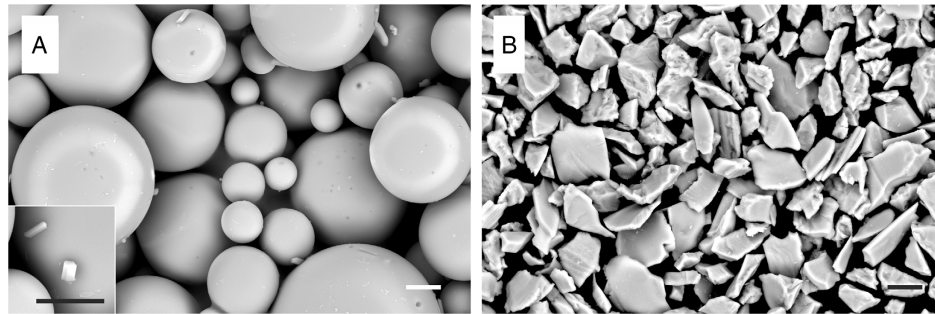
Figure 1. SEM images of A) spherical glass beads (insert of adherent smaller glass particles) and B) angular corundum particles applied for microblasting of FeMnCS LPBF-processed stents. Scale bars equal 10 μm.

roughness at the microscale regarding R_q and arithmetic average roughness (R_a) following DIN EN ISO 4287:2010[47] and stent strut width. The surface morphologies of the three different samples were observed by SEM (Leo 1530 Gemini, Zeiss).

Microcomputed tomography (μ-CT) was conducted with a Phoenix Nanotom M (General Electrics) at a tube current of 100 μA, a tube voltage of 100 kV, and a scan time of 30 min. While scanning the sample, 1000 absorption images were captured during a 360° rotation of the sample taken at discrete angular positions with an exposure time of $t = 0.5$ s. The voxel size was 7 μm. The resulting images were segmented using ScanIP (Synopsys Inc.) segmentation software, for visual inspection of surface topology at the macroscale. Thereby, none of the software's built-in numerical smoothing algorithms for surface smoothing have been employed to not alter surface topographies, such that the visible surface roughness in the 3D models is limited only by the resolution of the underlying μ-CT modality. The geometries in **Figure 2** will be used to build 3D computational mechanics models of stents at a later stage of the project,

to assess influences of surface topography, stent geometry and anisotropic material properties due to the LPBF scan directions relative to the stent struts on the mechanical performance of personalized stents.

The elemental composition of the treated stent surfaces was determined by energy-dispersive X-ray spectroscopy (EDX; Xflash4010, Bruker).

Primary human vascular SMC were isolated from the nondiseased part of the carotid artery obtained from a patient receiving carotid-subclavian bypass prior to aortic endovascular repair. The study was approved by the ethics committee of the Technische Universität Dresden (EK 151 042 017). Informed consent was obtained from each patient. Segments (1–2 mm³) were placed in Smooth Muscle Cell Growth Medium-2 with all supplements (SmGM-2, Lonza, CC-3182) with 10% heat-inactivated FBS (1.35 mL per 10 segments). After adding 40 μL of 1 N NaOH, this solution was given into 1.3 mL Pure Col solution (Advanced Biometric, 5005) in a 60 mm dish. A gel was formed after 110 min at 37 °C, 4 mL of SmGM-2 was added, and the media
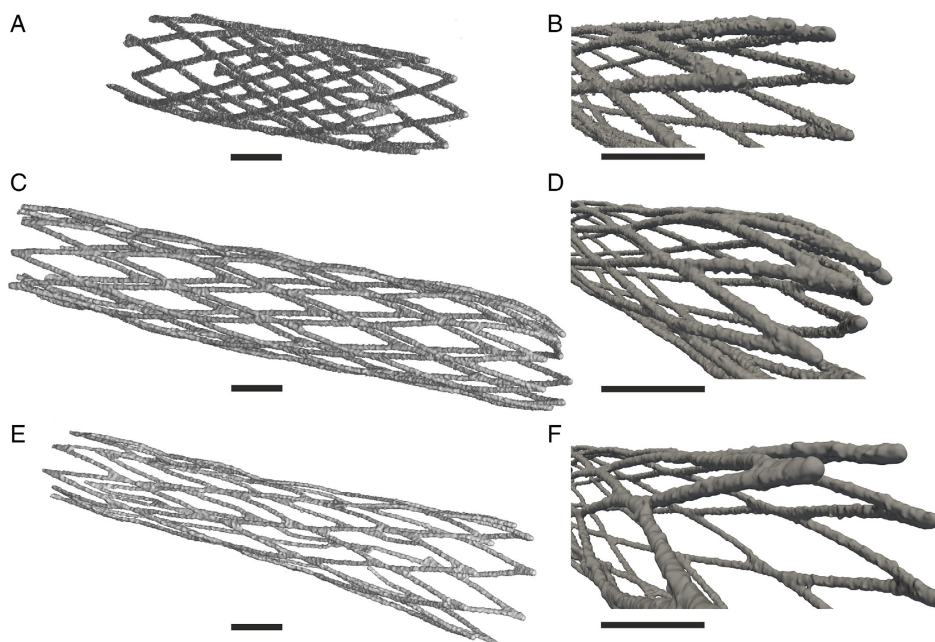
Figure 2. μ-CT-ablated 3D models of FeMnCS stents in A,B) as-built condition, after microblasting with C,D) glass beads and E,F) corundum particles. Scale bars equal 1 mm.
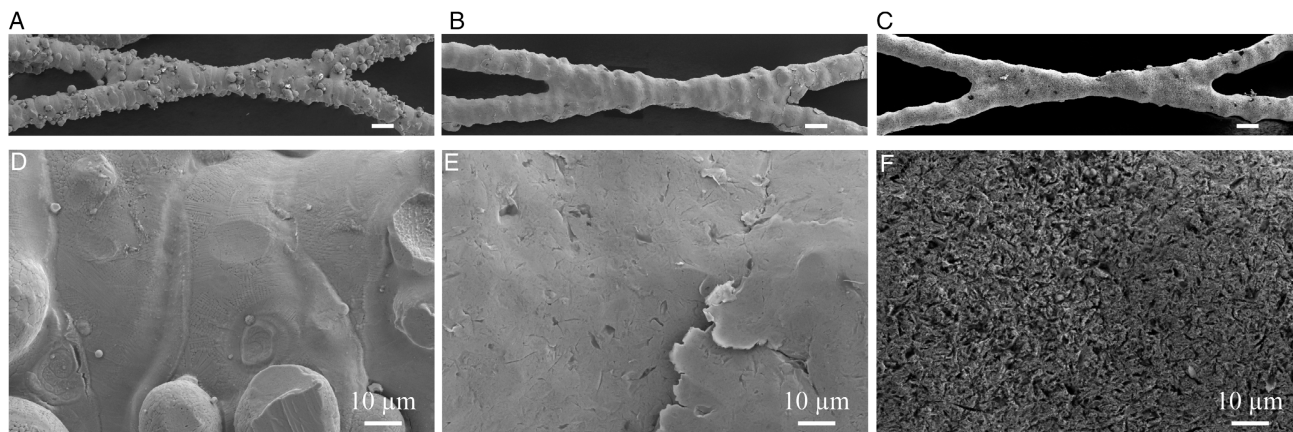
Figure 3. SEM images of stents in different conditions: A,D) as-built, after microblasting with B,E) glass beads and C,F) corundum. Upper scale bars equal 100 μm.

was changed twice a week. Outgrowing SMC were harvested by Collagenase I digestion of the gel and trypsin treatment of attached cells.

For adhesion of primary SMC, two rhombi of the stent structure (appr. 2 mg) were sterilized for 1 h under UV light. Afterward, 300 000 cells in 3 mL SmGM-2 were seeded onto stents placed in ultralow attachment plates (Corning, 3471). After 4 h, stents were carefully transferred into 100 mm dishes containing 20 mL SmGM-2 media. After 24 h, cell nuclei were stained with Hoechst 33 342 dye (0.2 mg mL^{-1}) for 20 min to monitor cell adhesion. Cells were fixed with paraformaldehyde and stained for alpha-smooth muscle actin (α-SMA) (1:100, Sigma-Aldrich, A5228) and phalloidin (1:100, Alexa Fluor 568, Invitrogen A12380). Alexa Fluor 488 goat antimouse IgG (4 μg mL^{-1}, Invitrogen, A11029) was used as a secondary antibody for α-SMA, and stent samples were documented using a Zeiss Axio Zoom (Carl Zeiss). SMC covered areas in relation to the total stent area were quantified by using Image J.[48] Effects were compared to samples of commercially available 316L stents (Boston Scientific).

3. Results and Discussion

In this study, a generic stent structure of FeMnCS was fabricated by LPBF having a relatively high surface roughness due to partially molten particles. However, a potential clinical application requires a smoother surface. As shown previously,[45] endothelial cells do not migrate onto process-immanent, therefore, larger partially molten particles and a removal of such particles or particle height reduction is necessary. One possibility is the mechanical process of microblasting, which is widely used for implants and very efficient.[49] Besides endothelial cells, SMC are in contact with the expanded stent in vivo, as well. A previous study demonstrated that the adhesion of SMC is also influenced by the topography of implant surfaces.[50] Therefore, a surface modification has to be established that promotes endothelial cell and simultaneously impedes SMC proliferation. This work focused on the interaction of SMC with two different modified stent surfaces.

3.1. Surface Characterization

In this study, LPBF-processed, biodegradable FeMnCS stents were either microblasted with spherical glass beads (Figure 1A) or angular corundum particles (Figure 1B) and compared with the as-built state, which was studied previously.[45] Those three modifications are presented in 3D models that were generated from μ-CT images (Figure 2). It is observable that roughness due to partially molten particles was reduced by microblasting. Furthermore, small deformations, at the end of the stent, became visible that can be traced back to the blasting treatment of individual stents and the manual handling for this purpose. This can be reduced by a respective treatment of the stents, when they are still fixed on the build plate. Further studies using microblasting are planned to reduce these deformations and to investigate the influence of microblasting on residual stresses and mechanical behavior.

Using SEM, a more detailed view on the stent struts is possible. In the as-built condition, partially molten particles were clearly visible, whereas microblasting reduced protruding particles (**Figure 3**A–C). Roughness measurements at the microscale confirmed these observations (**Table 2**). The root mean squared roughness (R_q) and arithmetic average roughness (R_a) of the microblasted stent strut surfaces were reduced from 3.17 ± 0.58 and 2.66 ± 0.58 μm for glass treatment and 2.88 ± 1.08 and 2.34 ± 0.86 μm for corundum treatment compared with the as-built surface 3.94 ± 0.77 and 3.27 ± 0.62 μm, respectively.[45] Conventional laser cut stents for cardiovascular applications need an arithmetic average roughness <0.5 μm,[51]

**Table 2.** Roughness of as-built stent struts and after microblasting with glass beads and corundum particles.

	R_q [μm]	R_a [μm]	R_q [μm] (by AFM)
As-built[45]	3.94 ± 0.77	3.27 ± 0.62	0.1183
Microblasted with glass beads	3.17 ± 0.58	2.66 ± 0.58	0.0885
Microblasted with corundum particles	2.88 ± 1.08	2.34 ± 0.86	0.1599

**ADVANCED
SCIENCE NEWS**

www.advancedsciencenews.com

*ADVANCED
ENGINEERING
MATERIALS*

www.aem-journal.com

which was not achieved by the microblasting in this study. However, a certain roughness for improved cell attachment or drug loading is necessary.[52,53] There are sandblasted 316L stents ($1.96 \pm 0.21\,\mu m$) commercially available,[53] which are used as polymer-free, drug-eluting stents. Therefore, corundum-treated

biodegradable stents ($R_a = 2.34 \pm 0.86\,\mu m$) might be an option for such application.

A different effect was revealed at the nanoscale (higher magnification of SEM images: Figure 3D–F) and was supported by AFM measurements (**Figure 4**). Corundum-treated surfaces have
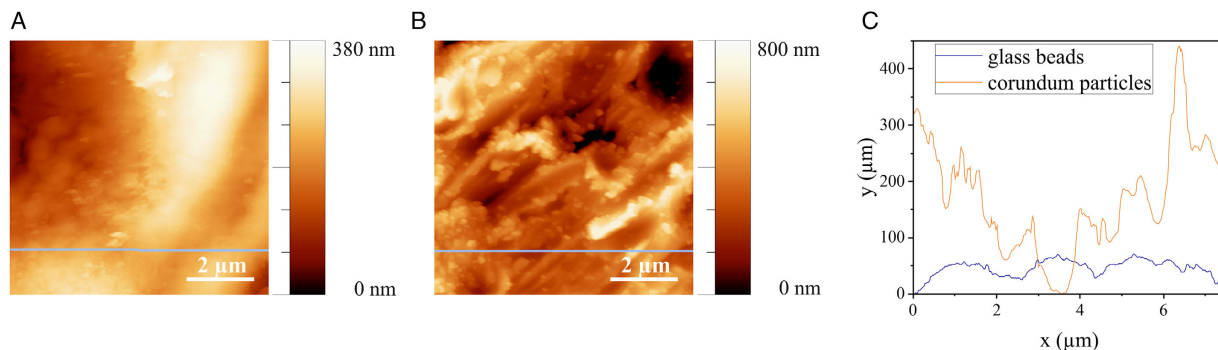
Figure 4. AFM topography images of FeMnCS stent surfaces after microblasting with A) glass beads and B) corundum and C) corresponding profiles of a line scan. Please note the differential scaling of the height images.
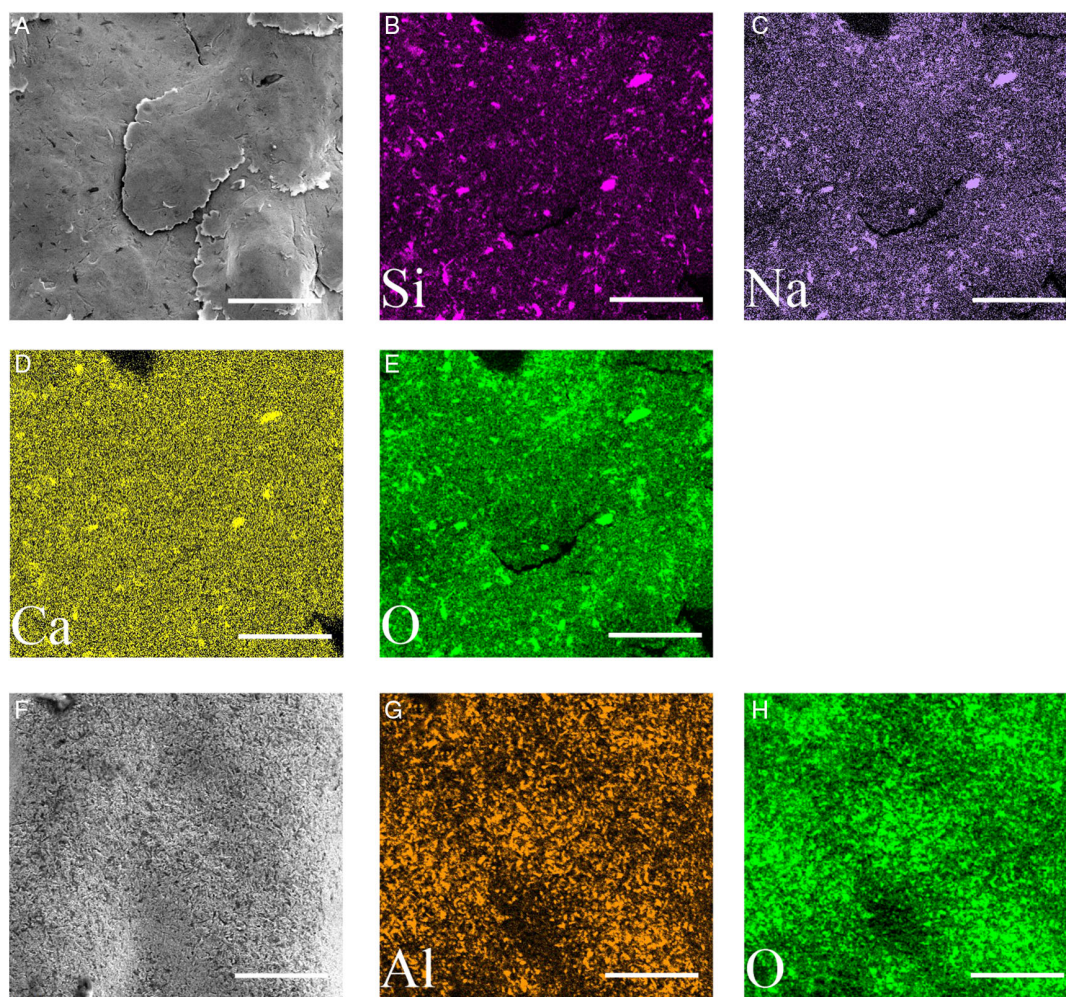
Figure 5. A) SEM image and B–E) related Si, Na, Ca, and O mappings of the FeMnCS stent surfaces after microblasting with glass beads. F) SEM image and G,H) related Al and O mappings of the FeMnCS stent surfaces after microblasting with corundum. Scale bars equal 50 μm.

a much higher R_q of 159.9 nm at the nanoscale compared to glass-treated surfaces (88.5 nm) since the irregular shaped corundum particles can strongly penetrate the surface. This could most likely increase the degradation rate, as seen for sandblasted Fe substrates[54] and will be investigated in more detail in ongoing studies. The conventional 316L stent, used as reference in this study, had a very smooth surface with an R_a of 7.889 nm. Furthermore, the stent strut width was decreased by the surface treatments, being $141.2 \pm 16.3 \, \mu m$ in the as-built state, and $134.5 \pm 9.5 \, \mu m$ in glass-treated to $115.7 \pm 8.2 \, \mu m$ in corundum-treated stents: increasingly strut material was ablated. A further reduction of the stent strut thickness is desirable, since it will reduce recirculation zones of the blood flow before and after the strut, which can eventually activate the coagulation cascade.[55,56]

EDX mappings after microblasting revealed a certain incorporation or deposition of the blasting material into the stent surfaces. For glass-treated surfaces (**Figure 5**A–E), small areas with higher concentrations of Si-, Na-, and Ca-oxides were detected, being the major components of the glass beads (Table 1). It is assumed that smaller particles adherent to the glass beads (Figure 1A insert) were pushed in the stent surface by larger glass beads. A similar behavior was observed for sandblasted Fe substrates, where Si signals were attributed to embedded SiC particles.[54] As Na- and Ca-ions are components of the blood plasma, their very small amounts will most likely not affect cells. It has been shown that Si-ions even enhance viability of endothelial cells.[57] Due to the treatment with corundum particles, Al-oxide was found on the stent surfaces (Figure 5F–H). Al-ions exert neurotoxicity and have no assigned biological function.[58] However, Al_2O_3 is a well-established bioinert material for orthopedic implants as well as blasting material for surface modification of dental implant systems, showing no harmful effects in these settings.[59,60]

3.2. Smooth Muscle Cell Adhesion and Morphology

In further experiments, the adhesion of primary SMC from the carotid artery to differentially treated surfaces was tested and compared to commercially available, corrosion resistant 316L stainless steel stents. The highest number of adherent cells was observed for the as-built state and the commercial 316L stent (**Figure 6**). The cells on the FeMnCS as-built stent showed a remarkable different randomized organization within the SMC orientation when compared to the well-structured flat population on the commercial 316L stent. This is also resulting in a lower area covered per cell (Figure 6E–H), and thereby in a higher cell density (number of nuclei; Figure 6I–L). Furthermore, surfaces after microblasting with glass beads and corundum exhibited a significant lower cell coverage. In contrast to the 316L stents, which SMC coverage could be described as flat, elongated and typical vessel-like, the FeMnCS stents showed a higher height profile, randomized orientation, and irregular nuclei morphology (**Figure 7**). The higher height profile and subsequent lower adhesion area per cell might be a sign for the lower ability to adhere to the FeMnCS stents surfaces. This effect was even more pronounced on the microblasted surfaces. The irregular nuclei morphology, especially observed in the treated surfaces, can hint to ongoing cell death, i.e., necrosis or apoptosis, and needs further clarification.
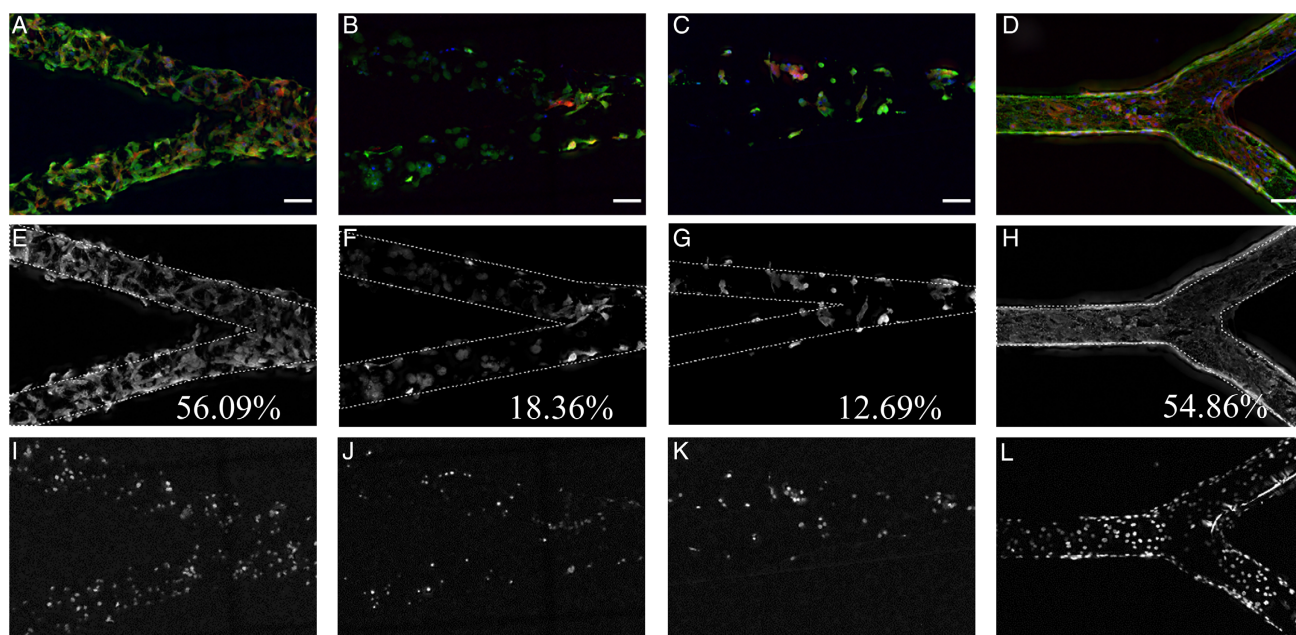
Figure 6. Attachment of primary smooth muscle cells on LPBF-manufactured FeMnCS stents in the A) as-built state and after microblasting with B) glass beads and C) corundum. D) Conventional 316L stents served as control. Primary SMC were isolated from the carotid artery and seeded in passage 5 on generic stents with different surface treatments. After 24 h SMC were fixed in paraformaldehyde and stained for α-SMA (green) and F-actin filaments with phalloidin (red). E–H) Determination of the α-SMA-positive areas in % within the region of interest (dotted lines). I–L) Cell nuclei were stained with Hoechst 33 342 dye to visualize cell density differences. Compared with the conventional 316L stent, FeMnCS as-built stents showed a lower degree of organization within the SMC orientation. Scale bars equal 100 μm.
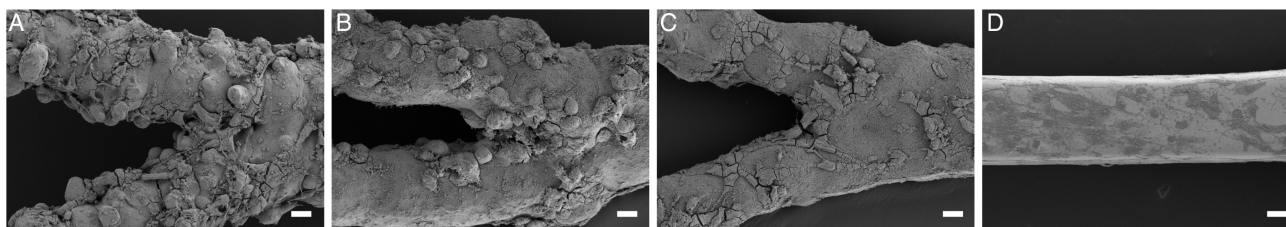
Figure 7. Analysis of the surface–SMC–interactions. SEM images of SMC attached to stent structures, A–C) FeMnCS manufactured by LPBF in comparison to D) conventional 316L stents. A) As-built state and after microblasting with B) glass beads and C) corundum. Primary SMC were isolated from the carotid artery and seeded on generic stents with different surface treatments. Cells were fixed 24 h after seeding. Scale bars equal 30 µm.

A previously published study revealed effects of surface treatments on endothelial cells and smooth muscle cell adhesion.[61] Vascular cells are important for integration of the stent in the surrounding tissue. Due to this, adhesion of endothelial cells and SMC should be initially favored.[61] However, adhesion and proliferation of endothelial cells are more important because a functional endothelial cell layer is antithrombogenic and antiproliferative, hence ISR or ST will be prevented. Previous studies have already demonstrated successful endothelial cell adhesion on such as-built surfaces.[45] In contrast, less adhesion of SMC is beneficial due to effects on migration and proliferation thus ISR would not be activated. A lower adhesion of SMC has been demonstrated for other surface modifications on metal stents and was seen positive.[30,62,63] However, it has been shown that an increasing surface roughness from 0.1 to 2 µm reduces SMC proliferation on biodegradable Mg-based stents in vitro.[46] In addition, in vivo studies demonstrated that a smooth and polished stent surface (arithmetic average roughness of about 40 nm) resulted in a decreased thrombus formation and neointimal hyperplasia compared to a rough stent (arithmetic average roughness of about 140 nm).[64,65] In further studies, the influence of microblasting on proliferation and migration rates of endothelial as well as SMC has to be analyzed to gain more insights, since the roughness of 88.5 and 159.9 nm at the nanolevel for biodegradable FeMnCS stents microblasted with glass beads and corundum particles, respectively, is not too far away to clinically applied stent roughness.

4. Conclusions

In summary, this study demonstrated that the microblasting with either glass beads or corundum particles of novel biodegradable Fe-based stents affected their surface roughness, stent morphology, surface elemental composition, and the adhesion of primary SMC. The microblasting treatment clearly decreased the roughness, whereby the roughness at the nanoscale of stents after microblasting with corundum particles is higher due to a stronger penetration of angular corundum particles.

It is important to note that the surface treatment with glass beads or corundum particles caused effects on SMC attachment with additional changes in cell morphology as seen in the as-built state. A lowering in smooth muscle cell adhesions might be beneficial in preventing ISR. Further studies are needed to analyze cell proliferation, migration, and viability of SMC. Finally, effects of the surface treatment on degradation rates, smooth muscle,

and endothelial cell physiology have to be addressed in the future.

Conflict of Interest

The authors declare no conflict of interest.

Data Availability Statement

The data that support the findings of this study are available from the corresponding author upon reasonable request.

[1] A. Zadpoor, J. Malda, *Ann. Biomed. Eng.* **2017**, *45*, 1.
[2] S. L. Sing, J. An, W. Yeong, F. Wiria, *J. Orthop. Res.* **2013**, *34*, 369.
[3] M. Tilton, G. Lewis, H. Bok Wee, A. Armstrong, M. Hast, G. Manogharan, *Addit. Manuf.* **2020**, *33*, 101137.
[4] P. Bajaj, A. Hariharan, A. Kini, P. Kürnsteiner, D. Raabe, E. A. Jägle, *Mater. Sci. Eng., A* **2020**, *772*, 138633.
[5] G. Li, E. Brodu, J. Soete, H. Wei, T. Liu, T. Yang, W. Liao, K. Vanmeensel, *Addit. Manuf.* **2021**, *47*, 102210.
[6] L.-C. Zhang, H. Attar, *Adv. Eng. Mater.* **2016**, *18*, 463.
[7] S. L. Sing, *Int. J. Bioprint.* **2022**, *8*, 478.
[8] J.-M. Seiz, K. Collier, E. Wulf, D. Bormann, F.-W. Bach, *Adv. Eng. Mater.* **2011**, *13*, B313.
[9] V. P. M. Rabeeh, T. Hanas, *Prog. Biomater.* **2022**, *11*, 163.
[10] P. Wen, M. Voshage, L. Jauer, Y. Chen, R. Poprawe, J. H. Schleifenbaum, *Mater. Des.* **2018**, *155*, 36.
[11] Y. Qin, P. Wen, H. Guo, D. Xia, Y. Zheng, L. Jauer, R. Poprawe, M. Voshage, J. H. Schleifenbaum, *Acta Biomater.* **2019**, *98*, 3.

[12] Y. Zheng, X. Gu, F. Witte, *Mater. Sci. Eng., R* **2014**, *77*, 1.

[13] Y. Yun, Z. Dong, N. Lee, Y. Liu, D. G. X. Xue, J. Kuhlmann, A. Doepke, H. Halsall, W. Heinemann, S. Sundaramurhty, M. Schulz, Z. Yin, V. Shanov, D. Hurd, P. Nagy, W. Li, *Mater. Today* **2009**, *12*, 22.

[14] F. Bär, L. Berger, L. Jauer, G. Kurtuldu, R. Schäublin, J. H. Schleifenbaum, J. F. Löffler, *Acta Biomater.* **2019**, *98*, 36.

[15] T. Niendorf, F. Brenne, P. Hoyer, D. Schwarze, M. Schaper, R. Grothe, M. Wiesener, G. Grundmeier, H. J. Maier, *Metall. Mater. Trans. A* **2015**, *46*, 2829.

[16] M. Montani, A. G. Demir, E. Mostaed, M. Vedani, B. Previtali, *Rapid Prototyping J.* **2017**, *23*, 514.

[17] C. Wang, Y. Shuai, Y. Yang, D. Zeng, X. Liang, S. Peng, C. Shuai, *J. Alloys Compd.* **2022**, *897*, 163247.

[18] J. Hufenbach, J. Sander, F. Kochta, S. Pilz, A. Voss, U. Kühn, A. Gebert, *Adv. Eng. Mater.* **2020**, *22*, 2000182.

[19] K. Lietaert, A. Zadpoor, M. Sonnaert, J. Schrooten, L. Weber, A. Mortensen, J. Vleugels, *Acta Biomater.* **2020**, *110*, 289.

[20] M. Otto, S. Pilz, A. Gebert, U. Kühn, J. Hufenbach, *Metals* **2021**, *11*, 944.

[21] T. Krüger, K.-P. Hoyer, V. Filor, S. Pramanik, M. Kietzmann, J. Meißner, M. Schaper, *J. Alloys Compd.* **2021**, *871*, 159544.

[22] M. Schinhammer, I. Gerber, A. C. Hänzi, P. J. Uggowitzer, *Mater. Sci. Eng., C* **2013**, *33*, 782.

[23] H. Hermawan, *Prog. Biomater.* **2018**, *7*, 93.

[24] M. Schinhammer, A. C. Hänzi, A. F. Löffler, P. J. Uggowitzer, *Acta Biomater.* **2010**, *6*, 1705.

[25] H. Hermawan, D. Dubé, D. Mantovani, *Acta Biomater.* **2010**, *6*, 1693.

[26] I. Andreou, P. I. I. Stone, D. Alexopoulos, M. Sabate, *Hellenic J. Cardiol.* **2020**, *61*, 9.

[27] E. Edelmann, C. Rogers, *Am. J. Cardiol.* **1998**, *81*, 4E.

[28] C. Chaabane, F. Otsuka, R. Vermani, M.-L. Bochaton-Piallat, *Cardiovasc. Res.* **2013**, *99*, 353.

[29] S. Marx, H. Totary-Jain, A. Marks, *Circ.: Cardiovasc. Interventions* **2011**, *4*, 104.

[30] G. Alexander, P. Hwang, J. Chen, J. Kim, B. Brott, Y. Yoon, H.-W. Jun, *ACS Biomater. Sci. Eng.* **2018**, *4*, 107.

[31] S. Bagherifard, N. Beretta, S. Monti, M. Riccio, M. Bandini, M. Guagliano, *Mater. Des.* **2018**, *145*, 28.

[32] S. Bagehorn, J. Wehr, H. Maier, *Int. J. Fatigue* **2017**, *102*, 135.

[33] J. Sun, M. Guo, K. Shi, D. Gu, *Mater. Sci. Add. Manuf.* **2022**, *1*, 11.

[34] M. Yang, Y. Shuai, Y. Youwen, D. Zeng, S. Peng, Z. Tian, C. Shui, *Virtual Phys. Prototyping* **2022**, *17*, 700.

[35] D. Obilanade, C. Dordlofva, P. Törlind, *Proc. Des. Soc.* **2021**, *1*, 2841.

[36] E. Maleki, S. Bagherifard, M. Bandini, M. Guagliano, *Addit. Manuf.* **2021**, *37*, 101619.

[37] I. Echeta, X. Feng, B. Dutton, R. Leach, S. Piano, *Int. J. Adv. Manuf. Technol.* **2020**, *106*, 2649.

[38] X. Gong, D. Zeng, W. Groeneveld-Meijer, G. Manogharan, *Mater. Sci. Add. Manuf.* **2022**, *1*, 6.

[39] B. Mehta, E. Hryha, L. Nyborg, F. Tholence, E. Johansson, *Metals* **2021**, *11*, 1070.

[40] P. Wen, Y. Qin, Y. Chen, M. Voshage, L. Jauer, R. Poprawe, J. Schleifenbaum, *J. Mater. Sci. Technol.* **2019**, *35*, 368.

[41] A. H. Maamoun, M. A. Elbestawi, S. C. Veldhuis, *J. Manuf. Mater. Process.* **2018**, *2*, 40.

[42] C. Maucher, P. Cera, H.-C. Möhring, *Procedia CIRP* **2022**, *108*, 560.

[43] J. Hufenbach, H. Wendrock, F. Kochta, U. Kühn, A. Gebert, *Mater. Lett.* **2017**, *186*, 330.

[44] J. Hufenbach, F. Kochta, H. Wendrock, A. Voß, L. Giebeler, S. Oswald, S. Pilz, U. Kühn, A. Lode, M. Gelinsky, A. Gebert, *Mater. Des.* **2018**, *142*, 22.

[45] B. Paul, A. Lode, A.-M. Placht, A. Voß, S. Pilz, U. Wolff, S. Oswald, A. Gebert, M. Gelinsky, J. Hufenbach, *ACS Appl. Mater. Interfaces* **2022**, *14*, 439.

[46] K. Zhou, Y. Li, L. Zhang, L. Jin, F. Yuan, J. Tan, G. Yuan, J. Pei, *Bioact. Mater.* **2021**, *6*, 262.

[47] German Institute for Standardization, *Geometrical Product Specifications - Surface Texture: Profile Method - Terms, Definitions and Surface Texture Parameters*, DIN EN ISO 4287:2010, Berlin, Germany **2010**.

[48] C. Schneider, W. Rasband, K. Eliceiri, *Nat. Methods* **2012**, *9*, 671.

[49] S. Lv, H. Tao, Y. Hong, Y. Zheng, C. Zhou, J. Zheng, L. Zhang, *Mater. Res. Express* **2019**, *6*, 106518.

[50] V. Taneja, A. Vertegel, E. Langan III, M. LaBerge, *Ann. Vasc. Surg.* **2011**, *25*, 675.

[51] E. Langi, L. Zhao, P. Jamshidi, M. Attallah, V. Silberschmidt, H. Willcock, F. Vogt, *J. Mater. Eng. Perform.* **2021**, *30*, 696.

[52] D. Khang, J. Lu, C. Yao, K. Haberstroh, T. Webster, *Biomaterials* **2008**, *29*, 970.

[53] R. Wessely, J. Hausleiter, C. Michaelis, B. Jaschke, M. Vogeser, S. Milz, B. Behnisch, T. Schratzenstaller, M. Renke-Gluszko, M. Stöber, E. Wintermantel, A. Kastrati, A. Schömig, *Arterioscler., Thromb., Vasc. Biol.* **2005**, *25*, 748.

[54] J. Zhou, Y. Yang, M. A. Frank, R. Detsch, A. Boccaccini, S. Virtanen, *ACS Appl. Mater. Interfaces* **2016**, *8*, 26482.

[55] J. Jimenez, P. Davies, *Ann. Biomed. Eng.* **2009**, *37*, 1483.

[56] A. Kastrati, J. Mehilli, J. Dirschinger, F. Dotzer, H. Schühlen, F.-J. Neumann, M. Fleckenstein, C. Pfafferott, M. Seyfarth, A. Schömig, *Circulation* **2001**, *103*, 2816.

[57] B. O'Brien, H. Zafar, A. Ibrahim, J. Zafar, F. Sharif, *Ann. Biomed. Eng.* **2016**, *44*, 523.

[58] S. C. Bondy, *NeuroToxicology* **2010**, *31*, 575.

[59] F. Zivic, S. Affatato, M. Trajanovic, M. Schnabelrauch, N. Grujovic, K. Choy, *Biomaterials in Clinical Practice - Advances in Clinical Research and Medical Devices*, Springer International Publishing AG, Cham, Switzerland **2018**.

[60] P. Schupbach, R. Glauser, S. Bauer, *Int. J. Biomater.* **2019**, *2*, article no. 6318429.

[61] S. Choudhary, M. Berhe, K. Haberstroh, T. Webster, *Int. J. Nanomed.* **2006**, *1*, 41.

[62] Z. Yang, X. Zhao, R. Hao, Q. Tu, X. Tian, Y. Xiao, K. Xiong, M. Wang, Y. Feng, N. Huang, G. Pan, *Proc. Natl. Acad. Sci.* **2020**, *117*, 16127.

[63] R. Hou, J. Wu, J. Wang, Z. Yang, A. Tu, X. Zhang, N. Huang, *Biomolecules* **2019**, *9*, 69.

[64] I. De Scheerder, J. Sohier, K. Wang, E. Verbeken, X. Zhou, L. Foyen, J. Van Humbeeck, J. Piessens, F. Van De Werf, *J. Interventional Cardiol.* **2000**, *13*, 179.

[65] I. De Scheerder, J. Sohier, E. Verbeken, L. Froyen, J. Van Humbeeck, *Materialwiss. Werkstofftech.* **2001**, *32*, 142.